applied sciences

MDPI

Article

Efficient Parallel FDTD Method Based on Non-Uniform Conformal Mesh

Kaihui Liu [1], Tao Huang [1], Liang Zheng [2], Xiaolin Jin [1,*], Guanjie Lin [1], Luo Huang [1], Wenjing Cai [1], Dapeng Gong [1] and Chunwang Fang [1]

[1] School of Electronic Science and Engineering, University of Electronic Science and Technology of China, Chengdu 610054, China; liukaihui@std.uestc.edu.cn (K.L.); huangtao@uestc.edu.cn (T.H.); linguanjie@std.uestc.edu.cn (G.L.); m18358944586@163.com (L.H.); 18200182991@163.com (W.C.); gongdapeng@uestc.edu.cn (D.G.); fangchunwang163@163.com (C.F.)

[2] National Supercomputing Center in Chengdu, Chengdu 610213, China; liangzh.cug@gmail.com

* Correspondence: jinxiaolin@uestc.edu.cn

Abstract: The finite-difference time-domain (FDTD) method is a versatile electromagnetic simulation technique, widely used for solving various broadband problems. However, when dealing with complex structures and large dimensions, especially when applying perfectly matched layer (PML) absorbing boundaries, tremendous computational burdens will occur. To reduce the computational time and memory, this paper presents a Message Passing Interface (MPI) parallel scheme based on non-uniform conformal FDTD, which is suitable for convolutional perfectly matched layer (CPML) absorbing boundaries, and adopts a domain decomposition approach, dividing the entire computational domain into several subdomains. More importantly, only one magnetic field exchange is required during the iterations, and the electric field update is divided into internal and external parts, facilitating the synchronous communication of magnetic fields between adjacent subdomains and internal electric field updates. Finally, unmanned helicopters, helical antennas, 100-period folded waveguides, and 16 × 16 phased array antennas are designed to verify the accuracy and efficiency of the algorithm. Moreover, we conducted parallel tests on a supercomputing platform, showing its satisfactory reduction in computational time and excellent parallel efficiency.

Keywords: FDTD; non-uniform conformal mesh; CPML absorption boundary; MPI parallel

check for updates

Citation: Liu, K.; Huang, T.; Zheng, L.; Jin, X.; Lin, G.; Huang, L.; Cai, W.; Gong, D.; Fang, C. Efficient Parallel FDTD Method Based on Non-Uniform Conformal Mesh. *Appl. Sci.* **2024**, *14*, 4364. https://doi.org/10.3390/app14114364

Academic Editor: Suchao Xie

Received: 20 April 2024
Revised: 11 May 2024
Accepted: 16 May 2024
Published: 21 May 2024

1. Introduction

The FDTD method, pioneered by Yee in 1966 [1], is well known as a seminal contribution in computational electromagnetics. Renowned for its succinct principle and ease of implementation, FDTD operates as a fully explicit algorithm devoid of matrix formulations, rendering it adept at accommodating intricate structures and anisotropic materials. It has found extensive utility across diverse electromagnetic phenomena, including transmission, radiation, and scattering.

One disadvantage of the traditional FDTD algorithm is that the use of uniform Cartesian mesh to discretize the computation domain results in a large number of grids. The non-uniform grid scheme [2] can simulate fine structures and reduce the number of grids. However, according to the Courant–Friedrichs–Lewy condition (CFL) [3], the maximum time step allowed is determined by the minimum mesh size of the computation domain, which means that the FDTD simulation must run a very large number of loops to reach a steady state. In addition, due to the step approximation adopted at the boundary of the model, not only will large errors be introduced, but sometimes false solutions will be obtained [4]. The mesh size needs to be reduced in order to reduce errors, which will inevitably increase the computational burden. To eliminate the problems caused by the stepwise approximation, Dey and Mittra proposed a conformal finite-difference time-domain (CFDTD) method [5], in which the cut-cell mesh can better approximate arbitrary surfaces and accurately simulate complex geometry [6] with second-order computational accuracy [7]. The CFDTD method can obtain the same calculation accuracy as traditional methods by using fewer grids, which has the advantages of high precision and high efficiency, and has been widely used and researched [6–9]. The combination of non-uniform and conformal mesh can greatly reduce the number of meshes and lower the amount of computation.

Another limitation of traditional FDTD algorithms is the additional computational burden of applying a PML based on physical models or a truncation of simulation regions. A PML enables the waves transmitted to the truncation to be absorbed by the boundary without reflection, thus simulating the propagation of the electromagnetic field in infinite space. At present, the widely used uniaxial perfectly matched layer (UPML) [10] and convolutional perfectly matched layer (CPML) [11] are improvements of the original PML algorithm [12] proposed in the 1990s, which can more accurately simulate the propagation behavior of waves in complex media and improve the accuracy and reliability of simulation results. However, the application of a PML usually increases the number of grids and the amount of computation, which inevitably raises the computation burden.

For FDTD methods based on non-uniform conformal grids and involving PML applications, the scale of problems that can be handled is severely limited by the available computing resources, and the rapid development of parallel computing provides solutions to the above problems. In particular, the FDTD method has a natural parallelism, which can solve large-scale problems on parallel platforms. For the moment, the parallel FDTD algorithm [13–17] has been widely implemented and tested on different computer platforms, among which the more commonly used field exchange method is to carry out one electric field exchange and one magnetic field exchange in the FDTD iteration process; the whole calculation process will be interrupted twice, and the processor will be idle and waiting when the electromagnetic field is transmitted. However, the field exchange method we adopted only needs one boundary magnetic field exchange while updating the internal electric field in the subregion, so that the transmission time and calculation time overlap, and the whole iteration process is interrupted only once, avoiding the waste of computing resources to a certain extent.

The present study integrates non-uniform conformal grids, MPI parallel techniques, and CPML absorption boundaries into the traditional FDTD algorithm. A series of computational experiments were conducted on a supercomputing platform to verify the accuracy and efficiency of the algorithm.

2. Theory and Methods

This section primarily discusses the fundamental theory of the non-uniform conformal FDTD method and the CPML absorbing boundary. Then, the MPI field exchange parallel scheme and program based on region decomposition are presented.

2.1. The Non-Uniform Conformal FDTD Algorithm

2.1.1. Internal Field Update

As shown in Figure 1, conformal grids are applied at the curved surface boundary of the object, where l_x and l_y represent the grid cell dimensions, excluding the perfect electric conductor (PEC) parts, and A_z denotes the grid cell area, excluding the PEC parts. The spatial distribution of the electromagnetic field components is consistent with the conventional Yee grid.

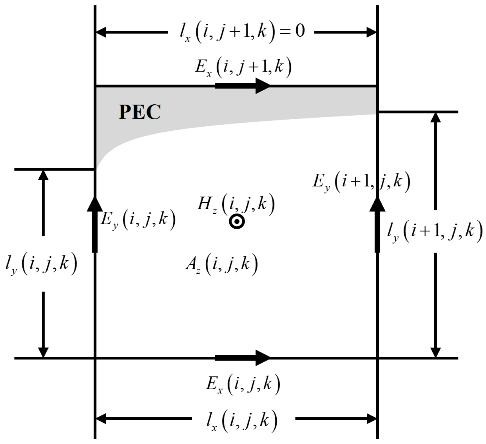

Figure 1. Schematic diagram of surface boundary conformal mesh.

The core idea of the conformal FDTD method is to replace the differential discretization equations with integral discretization equations based on Faraday's electromagnetic induction law at the conformal grid boundaries of the model [18], aiming to reduce errors caused by the discrete approximation of differential equations. The integral equation of Faraday's electromagnetic induction law is as follows:

$$\int_S \mu_0 \frac{\partial \vec{H}}{\partial t} \cdot d\vec{s} = -\oint_l \vec{E} d\vec{l} \tag{1}$$

Since the electromagnetic field inside the ideal metal is zero, the discrete loop integral of the electric field equals the electric field multiplied by the grid cell dimensions, excluding the ideal metal parts, and the integral of the magnetic field over the grid face equals the magnetic field multiplied by the area of the grid face, excluding the ideal metal parts. Taking the z-component as an example (other components follow a similar logic), the discrete formula for the magnetic field can be expressed as the following:

$$\begin{aligned} H_z^{n+\frac{1}{2}}(i+\frac{1}{2}, j+\frac{1}{2}, k) =& H_z^{n-\frac{1}{2}}(i+\frac{1}{2}, j+\frac{1}{2}, k) \\ &+ \frac{\Delta t}{\mu_0} \cdot \frac{1}{A_z(i+\frac{1}{2}, j+\frac{1}{2}, k)} \cdot \begin{bmatrix} -E_x^n(i+\frac{1}{2}, j, k) \cdot l_x(i+\frac{1}{2}, j, k) \\ +E_x^n(i+\frac{1}{2}, j+1, k) \cdot l_x(i+\frac{1}{2}, j+1, k) \\ -E_y^n(i+1, j+\frac{1}{2}, k) \cdot l_y(i+1, j+\frac{1}{2}, k) \\ +E_y^n(i, j+\frac{1}{2}, k) \cdot l_y(i, j+\frac{1}{2}, k) \end{bmatrix} \end{aligned} \tag{2}$$

The discrete update formula for the electric field component is consistent with the formula used in the FDTD method with non-uniform grids. Specifically,

$$\begin{aligned} E_z^{n+1}\left(i, j, k+\tfrac{1}{2}\right) = E_z^n\left(i, j, k+\tfrac{1}{2}\right) - \tfrac{\Delta t}{\varepsilon_0} \cdot \Bigg[& \tfrac{H_y^{n+1/2}\left(i+\frac{1}{2}, j, k+\frac{1}{2}\right) - H_y^{n+1/2}\left(i-\frac{1}{2}, j, k+\frac{1}{2}\right)}{h_{x_i}} \\ & - \tfrac{H_x^{n+1/2}\left(i, j+\frac{1}{2}, k+\frac{1}{2}\right) - H_x^{n+1/2}\left(i, j-\frac{1}{2}, k+\frac{1}{2}\right)}{h_{y_j}} \Bigg] \end{aligned} \tag{3}$$

where the edge length between non-uniform grid points is given by the following:

$$\begin{cases} \Delta x_i = x_{i+1} - x_i, i = 1, \cdots, N_x - 1 \\ \Delta y_j = y_{j+1} - y_j, j = 1, \cdots, N_y - 1 \\ \Delta z_k = z_{k+1} - z_k, k = 1, \cdots, N_z - 1 \end{cases} \tag{4}$$

The edge length in Formula (3) is given by the following:

$$\begin{cases} h_{x_i} = (\Delta x_i - \Delta x_{i-1})/2, i = 2, \cdots, N_x - 1 \\ h_{y_j} = (\Delta y_j - \Delta y_{j-1})/2, j = 2, \cdots, N_y - 1 \\ h_{z_k} = (\Delta z_k - \Delta z_{k-1})/2, k = 2, \cdots, N_z - 1 \end{cases} \tag{5}$$

2.1.2. Boundary Conditions

Common boundary conditions include the electric boundary, magnetic boundary, periodic boundary, PML, etc. Among them, the electric boundary, magnetic boundary, and periodic boundary are relatively easy to implement in parallel, while absorbing boundaries are more complex and widely used in radiation, scattering, and other problems. In this paper, CPML absorbing-boundary conditions are adopted, and a parallel scheme is provided.

Take the z-direction electric field component as an example (other components follow a similar logic). In stretched-coordinate space, the Maxwell's equations in the PML medium can be expressed as the following:

$$j\omega\varepsilon E_z = s_x^{-1}\frac{\partial H_y}{\partial x} - s_y^{-1}\frac{\partial H_x}{\partial y} \tag{6}$$

where the coordinate stretching factor is given by the following:

$$s_\eta = \kappa_\eta + \frac{\sigma_\eta}{\alpha_\eta + j\omega\varepsilon_0}, (\eta = x, y, z) \tag{7}$$

κ_η, σ_η, and α_η are positive real numbers, and $\kappa_\eta \geq 1$.

In order to integrate the CPML absorbing-boundary algorithm with the non-uniform conformal FDTD algorithm, the discrete formulation of the Maxwell's equations in the CPML medium is provided [19]. This involves replacing the differential discretization equation with the integral discretization equation of the Faraday's electromagnetic induction law for the CPML. The discrete formulation for the z-component of the electric field is given by the following:

$$\begin{aligned} E_z^{n+1}\left(i,j,k+\tfrac{1}{2}\right) = {} & \tfrac{2\varepsilon_r\varepsilon_0 - \sigma\Delta t}{2\varepsilon_r\varepsilon_0 + \sigma\Delta t} E_z^n\left(i,j,k+\tfrac{1}{2}\right) - \tfrac{2\Delta t}{2\varepsilon_r\varepsilon_0 + \sigma\Delta t} \cdot \\ & \left[\tfrac{H_y^{n+1/2}\left(i+\frac{1}{2},j,k+\frac{1}{2}\right) - H_y^{n+1/2}\left(i-\frac{1}{2},j,k+\frac{1}{2}\right)}{\kappa_x\left(i,j,k+\frac{1}{2}\right)h_{x_i}} \right. \\ & - \tfrac{H_x^{n+1/2}\left(i,j+\frac{1}{2},k+\frac{1}{2}\right) - H_x^{n+1/2}\left(i,j-\frac{1}{2},k+\frac{1}{2}\right)}{\kappa_y\left(i,j,k+\frac{1}{2}\right)h_{y_j}} \\ & \left. + \psi_{ezx}^{n+1/2}\left(i,j,k+\tfrac{1}{2}\right) - \psi_{ezy}^{n+1/2}\left(i,j,k+\tfrac{1}{2}\right) \right] \end{aligned} \tag{8}$$

$$\begin{aligned} \psi_{ezx}^{n+1/2}\left(i,j,k+\tfrac{1}{2}\right) = {} & b_x \psi_{ezx}^{n-1/2}\left(i,j,k+\tfrac{1}{2}\right) \\ & + a_x \tfrac{H_y^{n+1/2}\left(i+\frac{1}{2},j,k+\frac{1}{2}\right) - H_y^{n+1/2}\left(i-\frac{1}{2},j,k+\frac{1}{2}\right)}{h_{x_i}} \end{aligned} \tag{9}$$

$$\begin{aligned} \psi_{ezy}^{n+1/2}\left(i,j,k+\tfrac{1}{2}\right) = {} & b_y \psi_{ezy}^{n-1/2}\left(i,j,k+\tfrac{1}{2}\right) \\ & + a_y \tfrac{H_x^{n+1/2}\left(i,j+\frac{1}{2},k+\frac{1}{2}\right) - H_x^{n+1/2}\left(i,j-\frac{1}{2},k+\frac{1}{2}\right)}{\kappa_y\left(i,j,k+\frac{1}{2}\right)h_{y_j}} \end{aligned} \tag{10}$$

where

$$a_\eta = \frac{\sigma_\eta}{\sigma_\eta\kappa_\eta + \alpha_\eta\kappa_\eta^2}\left(e^{-(\sigma_\eta/\kappa_\eta + \alpha_\eta)\frac{\Delta t}{\varepsilon_0}} - 1\right), b_\eta = e^{-(\sigma_\eta/\kappa_\eta + \alpha_\eta)\frac{\Delta t}{\varepsilon_0}} \tag{11}$$

The update formula for the magnetic field component is replaced with the integral discretization form. The integral discretization formula for the z-component of the magnetic field is given by the following:

$$\begin{aligned} H_z^{n+1/2}\left(i+\tfrac{1}{2},j+\tfrac{1}{2},k\right) = {} & H_z^{n-1/2}\left(i+\tfrac{1}{2},j+\tfrac{1}{2},k\right)+\frac{\Delta t}{\mu_0 A_z\left(i+\frac{1}{2},j+\frac{1}{2},k\right)}\cdot \\ & \left[\frac{E_x^n\left(i+\frac{1}{2},j+1,k\right)\cdot l_x\left(i+\frac{1}{2},j+1,k\right)-E_x^n\left(i+\frac{1}{2},j,k\right)\cdot l_x\left(i+\frac{1}{2},j,k\right)}{\kappa_y\left(i+\frac{1}{2},j+\frac{1}{2},k\right)}\right. \\ & \left.-\frac{E_y^n\left(i+1,j+\frac{1}{2},k\right)\cdot l_y\left(i+1,j+\frac{1}{2},k\right)-E_y^n\left(i,j+\frac{1}{2},k\right)\cdot l_y\left(i,j+\frac{1}{2},k\right)}{\kappa_x\left(i+\frac{1}{2},j+\frac{1}{2},k\right)}\right] \\ & +\frac{\Delta t}{\mu_0}\left[\psi_{h_{zy}}^n\left(i+\tfrac{1}{2},j+\tfrac{1}{2},k\right)-\psi_{h_{zx}}^n\left(i+\tfrac{1}{2},j+\tfrac{1}{2},k\right)\right] \end{aligned} \tag{12}$$

$$\begin{aligned} \psi_{h_{zy}}^n\left(i+\tfrac{1}{2},j+\tfrac{1}{2},k\right) = {} & b_y\psi_{h_{zy}}^{n-1}\left(i+\tfrac{1}{2},j+\tfrac{1}{2},k\right) \\ & +a_y\frac{E_x^n\left(i+\frac{1}{2},j+1,k\right)\cdot l_x\left(i+\frac{1}{2},j+1,k\right)-E_x^n\left(i+\frac{1}{2},j,k\right)\cdot l_x\left(i+\frac{1}{2},j,k\right)}{A_z\left(i+\frac{1}{2},j+\frac{1}{2},k\right)} \end{aligned} \tag{13}$$

$$\begin{aligned} \psi_{hx}^n\left(i+\tfrac{1}{2},j+\tfrac{1}{2},k\right) = {} & b_x\psi_{h_{zx}}^{n-1}\left(i+\tfrac{1}{2},j+\tfrac{1}{2},k\right) \\ & +a_x\frac{E_y^n\left(i,j+\frac{1}{2},k\right)\cdot l_y\left(i,j+\frac{1}{2},k\right)-E_y^n\left(i+1,j+\frac{1}{2},k\right)\cdot l_y\left(i+1,j+\frac{1}{2},k\right)}{A_z\left(i+\frac{1}{2},j+\frac{1}{2},k\right)} \end{aligned} \tag{14}$$

Compared to other PML absorbing-boundary methods, CPMLs can be more easily parallelized, as Formulas (8) and (12) can be extended to the entire computational domain. When κ_x and κ_y are set to 1, and a_x, a_y, b_x, and b_y are set to 0, the field update equations degenerate into those of the non-PML region. Therefore, it is only necessary to precompute the field update coefficients for the PML and non-PML regions in MPI parallel computation, ensuring that the parallel processes for both regions of the FDTD algorithm are consistent, which effectively reduces parallel complexity.

2.2. MPI Field Exchange Technique

The principle of parallel computing is to decompose large-scale problems into smaller-scale ones that can be executed simultaneously using multiple processors. The FDTD algorithm is inherently suitable for parallelization because the update of field values at specific nodes depends only on the field values of their neighboring nodes, requiring the transmission of the necessary neighboring node field values.

This paper adopts a parallel FDTD method based on domain decomposition, where the entire computational domain is divided into numerous smaller subdomains and mapped onto independent processors on a parallel platform. Each processor now deals with the field calculations within its respective subdomain to alleviate the computational burden on a single processor. In the domain decomposition of parallel computing, to avoid unnecessary numerical interpolation, the interfaces between subdomains are consistent with the FDTD grid, and the MPI functions are used to transmit the required electromagnetic field components at the interfaces between subdomains.

Suppose the subdomains are arranged along one direction for brevity, with the x-direction being the example in this paper. As shown in Figure 2, the orange-colored face with the grid index i represent the interfaces between subdomains. A layer of virtual grid cells is used to facilitate the information exchange between the two subdomains. These virtual grid cells contain field information from adjacent subdomains. For instance, the virtual grid cell index in process N (marked by red lines) is (i, j, k), while in process N + 1 (marked by blue lines), it is $(i-1, j, k)$.The electric field components $E_{y,z}(i, j, k)$ and magnetic field components $H_x(i, j, k)$ at the interface are overlapping field components from two adjacent subdomains, and they need to be updated in both processes N and N + 1. The magnetic field component $H_{y,z}(i-1, j, k)$ updated in process N will be passed to process N + 1 to update the electric field component at the interface. Similarly, the magnetic field component $H_{y,z}(i,j,k)$ updated in process N + 1 will be passed to process N to update the electric field component at the interface.

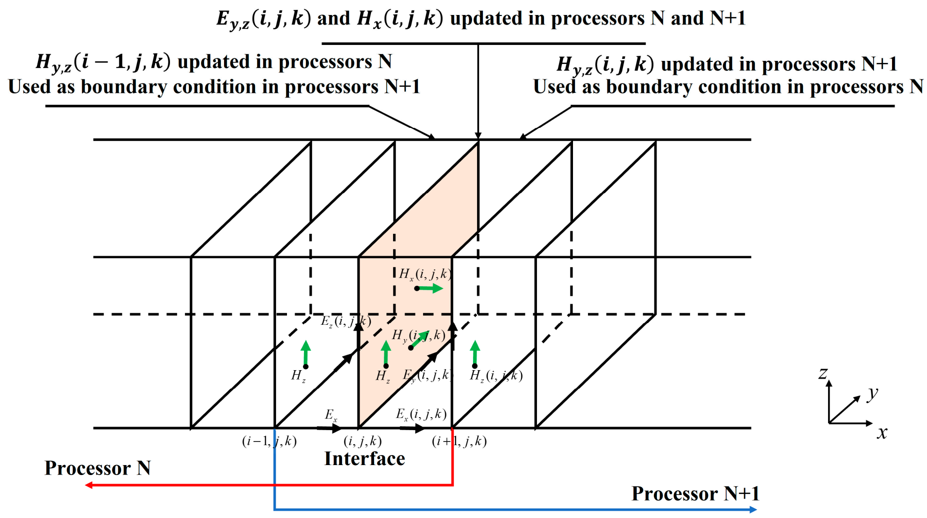

Figure 2. Schematic of field update at subdomain interfaces.

From the perspective of reliability in parallel programming and the application of non-uniform conformal grids, adding virtual grid cells offers significant advantages. If the interfaces between subdomains coincide with material interfaces, in addition to transmitting magnetic field information, it is also necessary to transmit relevant conformal grid information and material information. In this scheme, however, the electromagnetic fields, as well as the associated grid and material information, at the interfaces between subdomains, are all included within the current subdomain. This ensures that the field update information in each subdomain is readily available within its own domain.

Figure 3 depicts a three-dimensional schematic of the exchange of electromagnetic fields between adjacent subdomains. The orange markings denote the interface between the subdomains. The virtual mesh indices in processes N and N + 1 are $(nx+1,j,k)$ and $(0,j,k)$, respectively, which are used to store the magnetic field and conformal grid information from adjacent subdomains. It is only necessary to exchange the magnetic fields H_y and H_z at the interface between the two neighboring subdomains. The subdomains are interrupted only once in each iterative step.

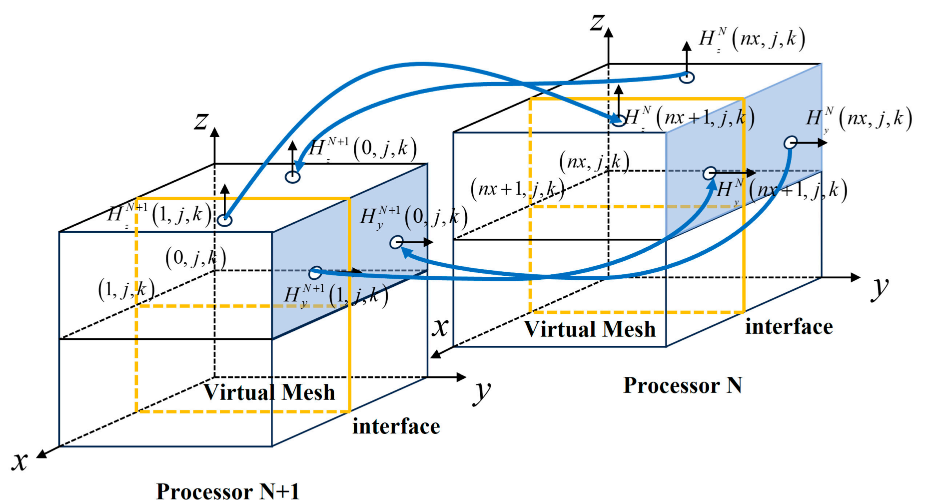

Figure 3. Three-dimensional schematic of electromagnetic field exchange between adjacent subdomains.

To minimize the impact of transmission time on the overall computation time, we adopted the scheme of separating the outermost layer of the subregion from the inner region [15], so the update of the electric field in each subdomain is divided into boundary updates and internal updates, as shown in Figure 4. The gray area represents the virtual grid, and the orange lines denote the interface. Since the transmission of the magnetic field mainly occurs at the boundaries of the subdomains, we can improve the parallel performance by overlapping internal computation with boundary magnetic field transmission. While performing a non-blocking transmission of boundary magnetic fields, the electric field within the subdomain is updated. After the transmission is completed, the boundary electric field is updated. This method allows the computation time for field updates to overlap with the transmission time, especially when there is a large amount of data to be transmitted for the boundary magnetic fields, resulting in a higher efficiency.

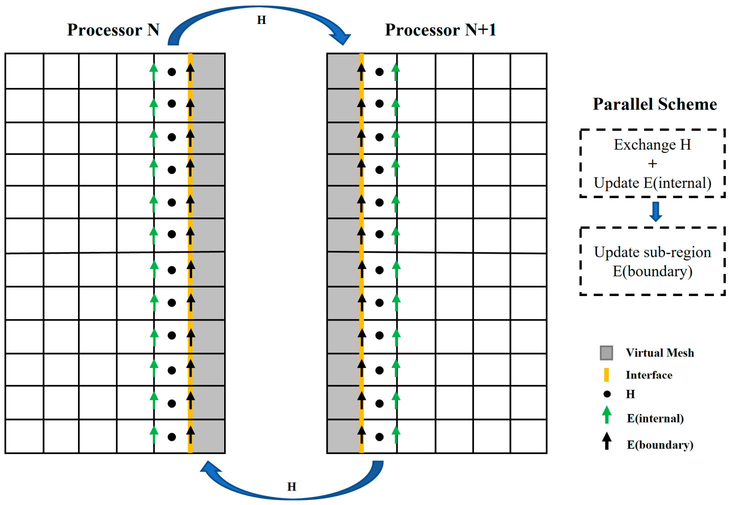

Figure 4. Schematic of overlapping between transmission of magnetic fields across adjacent subdomains and updating of internal electric fields.

3. Results

In this section, four simulation cases are conducted using simulations of an unmanned helicopter, a helical antenna, a 100-period folded waveguide, and a 16 $\times$ 16 phased array antenna. The parallel and serial results are compared, and the parallel efficiency is tested. All tests are performed on a supercomputing platform equipped with a 1 $\times$ 86 Hygon 7285 processor (Haiguang Information Technology Co., Ltd., Tianjin, China) with 32 cores operating at a 2.5 GHz frequency and 8 16 GB DDR4 2666 ECC REG memory modules per node.

3.1. Performance Analysis on Single Node

Firstly, we designed two test cases, an unmanned helicopter and a helical antenna, to evaluate the parallel performance on a single node. The models are shown in Figure 5a,b, respectively. The frequencies are set to 1.6–1.8 GHz and 0.2–1.0 GHz, and the excitations are plane wave excitation and waveguide port excitation, respectively. Gaussian signals are used for both cases. The computational domains are discretized into non-uniform conformal grids with dimensions of 7,468,047 (183 $\times$ 223 $\times$ 183) and 10,400,760 (173 $\times$ 334 $\times$ 180), respectively. Both cases adopt 15 layers of CPML absorbing-boundary conditions to truncate the computational domain's six boundaries.

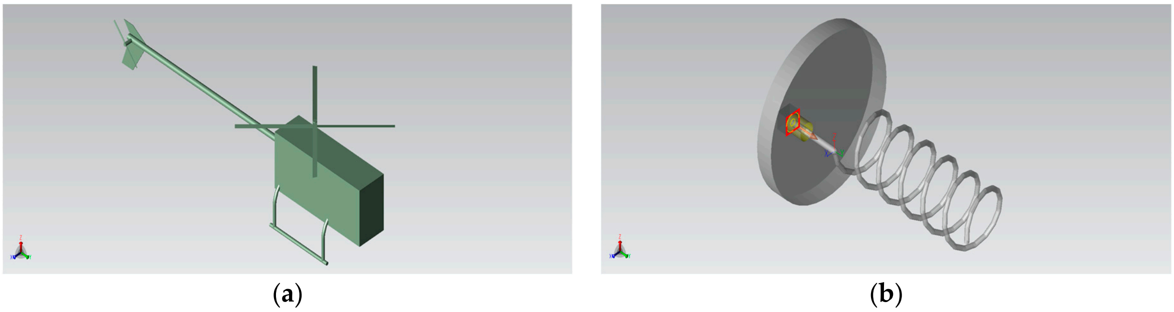

Figure 5. (**a**) Unmanned helicopter; (**b**) helical antenna.

As shown in Figure 6a–d, the far-field patterns of the unmanned helicopter and the helical antenna, respectively, show complete consistency between serial and parallel results, and are basically consistent with the CST results, indicating the correctness of the parallel algorithm results.

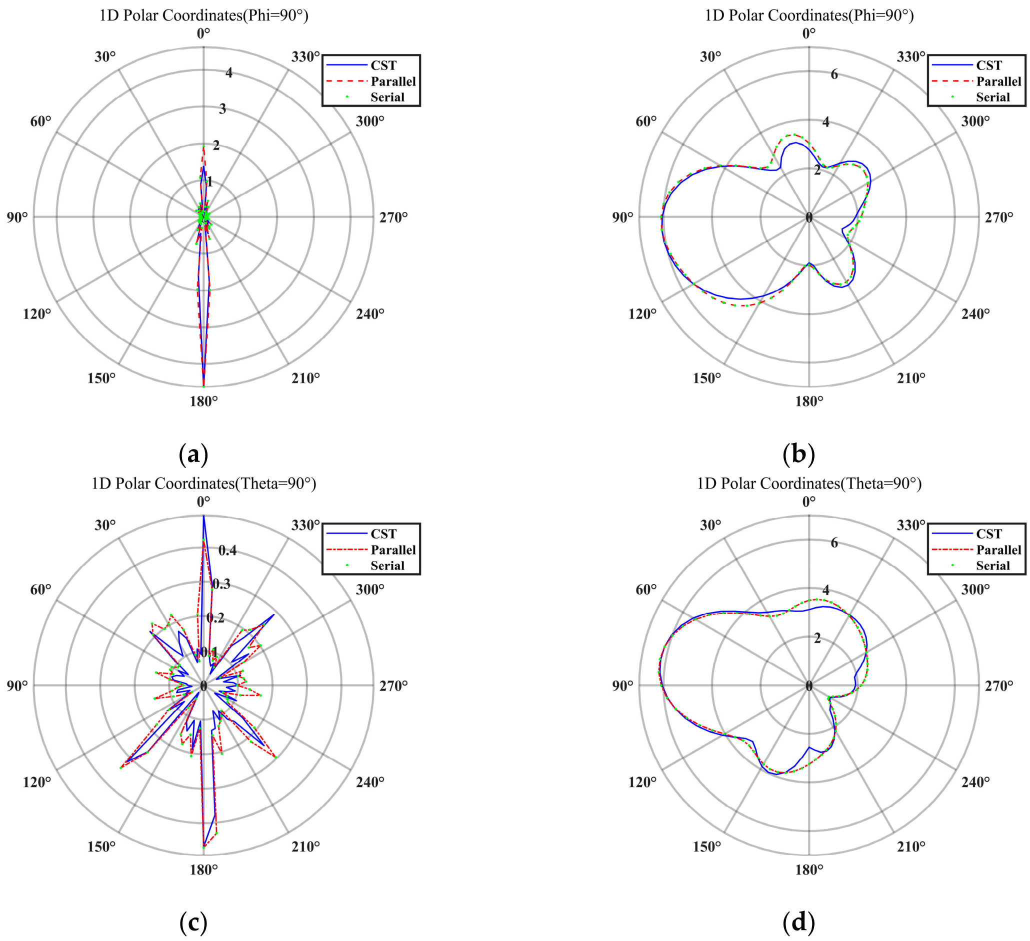

Figure 6. (**a**) Unmanned helicopter far-field pattern at phi = 90°; (**b**) helical antenna far-field pattern at phi = 90°; (**c**) unmanned helicopter far-field pattern at theta = 90°; (**d**) helical antenna far-field pattern at theta = 90°.

Tests were conducted on the supercomputing platform, with processors counts set to 1, 2, 4, 8, 12, and 16. Specific test data are provided in Table 1, and the scalability and efficiency are illustrated in Figure 7a,b. It can be observed that the parallel efficiency of both cases is above 90%, and the scalability approaches linearity. These test results demonstrate that the non-uniform conformal parallel FDTD algorithm performs well with a small number of processors on a single node, and it also presents excellent acceleration effects for CPML absorbing-boundary layers.

Table 1. Single-node parallel testing results table.

Processors	Unmanned Helicopter			Helical Antenna		
	Time(s)	Scalability	Efficiency (%)	Time(s)	Scalability	Efficiency (%)
1	148,714	1	100%	133,379	1	100%
2	75,172.8	1.98	98.9%	69,023	1.93	96.6%
4	38,031.1	3.91	97.8%	33,983.5	3.92	98.1%
8	19,596.8	7.59	94.9%	17,899.5	7.45	93.1%
12	13,397.6	11.10	92.5%	12,158.5	10.97	91.4%
16	10,313.0	14.42	90.1%	9192.2	14.51	90.7%

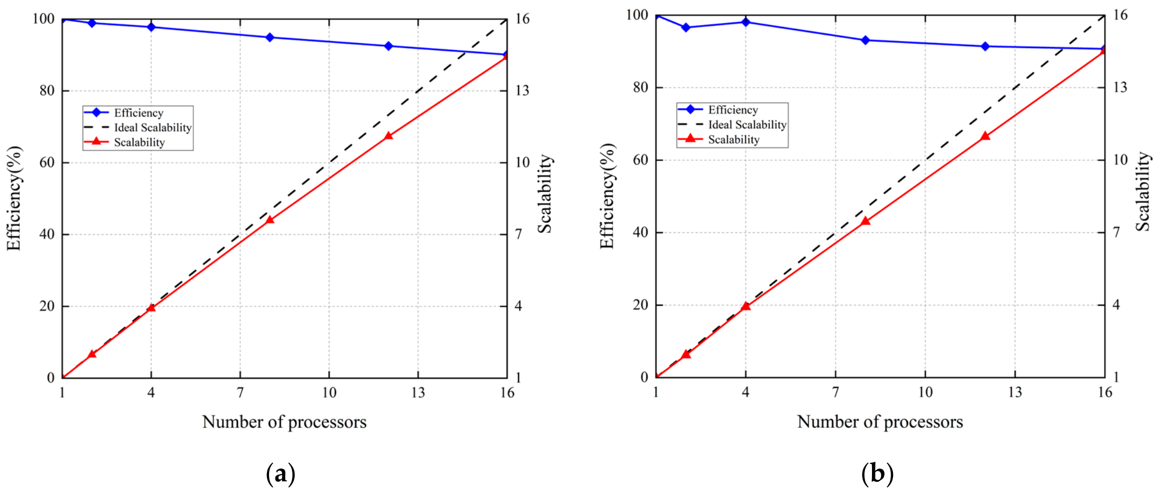

Figure 7. (**a**) The parallel scalability and efficiency of an unmanned helicopter on a single node; (**b**) the parallel scalability and efficiency of helical antenna on a single node.

3.2. Performance Analysis on Multi-Node

We conducted experiments utilizing two distinct scenarios: a 100-period folded waveguide and a 16 $\times$ 16 phased array antenna array, depicted in Figure 8a,b, respectively. These experiments were aimed at evaluating the algorithm's parallel efficacy across multiple computational nodes. The operating frequencies were set at 219–221 GHz and 4–5 GHz correspondingly, with excitation applied at the waveguide ports. Gaussian signals were adopted, and the computational domains were discretized into non-uniform conformal grids, sized at 41,277,600 (70 $\times$ 91 $\times$ 6480) and 33,808,320 (540 $\times$ 728 $\times$ 86), respectively. What is more, boundary conditions were enforced by using electric boundary and CPML absorbing techniques.

Figure 9 shows the S-parameter results of the folded waveguide, where S11 is completely below -15 dB and S21 is completely within -0.12 dB. Both our algorithm and CST show good transmission characteristics. Figure 10a,b depict the far-field patterns for the antenna array. The serial and parallel results are entirely consistent, and basically consistent with the CST results, also indicating the correctness of the parallel algorithm results.

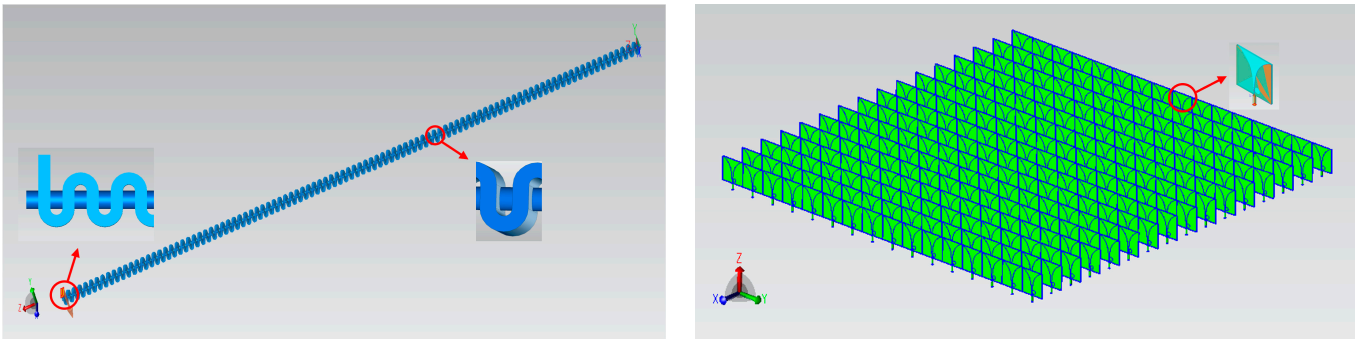

(a) (b)

Figure 8. (**a**) A 100-period folded waveguide; (**b**) a 16 × 16 phased array antenna.

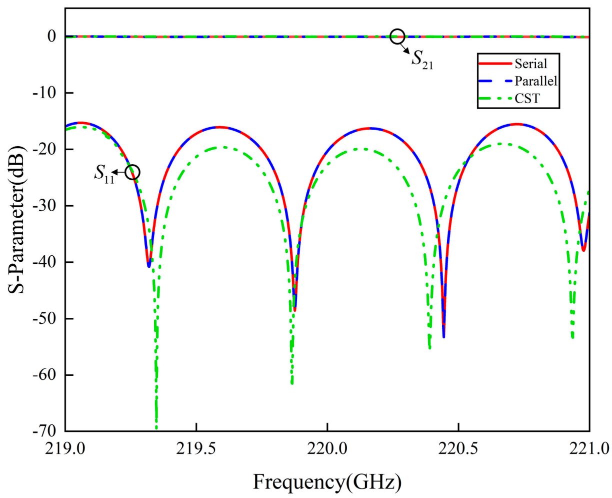

Figure 9. The S-parameter results of the 100-period folded waveguide.

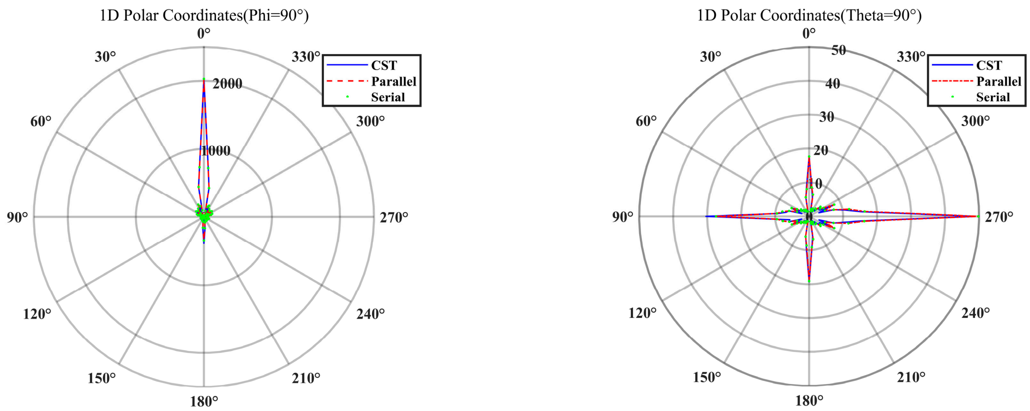

(a) (b)

Figure 10. (**a**) A 16 × 16 phased array antenna far-field pattern at phi = 90°; (**b**) a 16 × 16 phased array antenna far-field pattern at theta = 90°.

On the supercomputing platform, the parallel non-uniform conformal FDTD algorithm was executed with different numbers of processors ranging from 1 to 1024. The number of processors for domain decomposition was selected from 1 to 1024, including 1, 2, 4, 8, 16, 32, 64, 128, 256, 512, and 1024. Multi-node parallelism started with 64 processors, and 1024 processors were run on 33 nodes. The specific test data are provided in Table 2. From Figure 11, it can be observed that the computational time for both cases decreased significantly from 4,672,834 s and 996,042 s for single processors to 6264.5 s and 1316.3 s for 1024 processors, respectively, resulting in a substantial reduction in computation time.

Table 2. Muti-node parallel testing results table.

Processors	100-Period Folded Waveguide			16 × 16 Phased Array Antenna		
	Time(s)	**Scalability**	**Efficiency (%)**	**Time(s)**	**Scalability**	**Efficiency (%)**
1	4,672,834	1	100.00%	996,042	1	100.00%
2	2,352,144	1.99	99.3%	505,605	1.97	98.6%
4	1,211,352	3.86	96.4%	258,712	3.85	96.3%
8	613,031	7.62	95.3%	131,403	7.58	94.8%
16	308,052	15.17	94.8%	66,848.5	14.9	93.4%
32	164,602	28.39	88.7%	35,611.1	27.97	87.4%
64	84,938.1	55.01	86.0%	18,705.0	53.25	83.2%
128	50,349.4	92.81	72.5%	9717.5	102.5	80.1%
256	23,981.7	194.85	76.1%	4981.7	199.94	78.1%
512	12,190.1	383.33	74.9%	2573.3	387.07	75.6%
1024	6264.5	745.93	72.8%	1316.3	756.7	73.9%

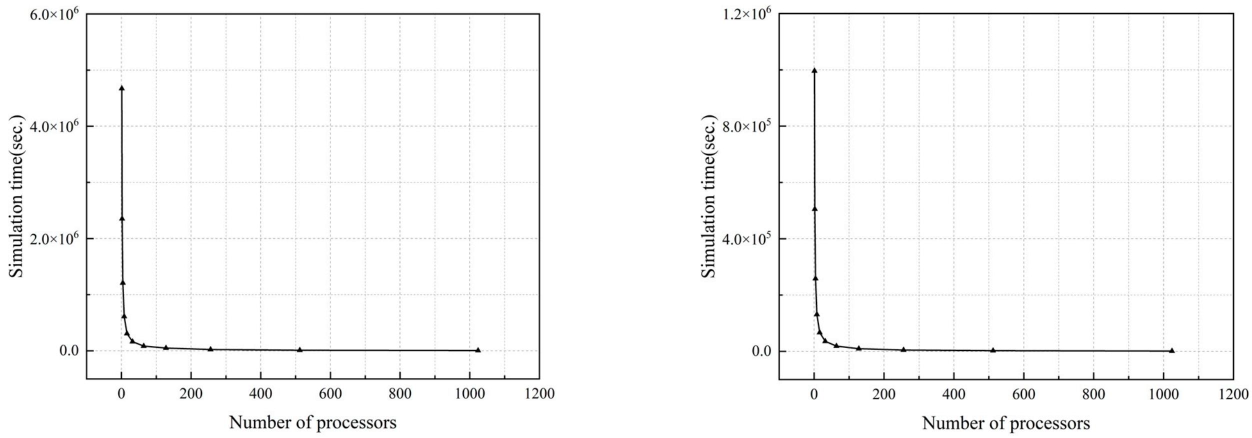

(**a**) (**b**)

Figure 11. (**a**) The time consumption of the 100-period folded waveguide; (**b**) the time consumption of the 16 × 16 phased array antenna.

The scalability and efficiency of the parallel non-uniform conformal FDTD algorithm are illustrated in Figure 12. The overall parallel efficiency for both cases is above 70%, reaching a maximum of 99.3% (with 2 processors) and a minimum of 72.8% (with 1024 processors). The efficiency can reach 90% with a small number of processors, and the scalability approaches linearity. However, as the number of processors increases, especially when cross-node communication is involved, the parallel efficiency gradually decreases, which is consistent with general parallel trends.

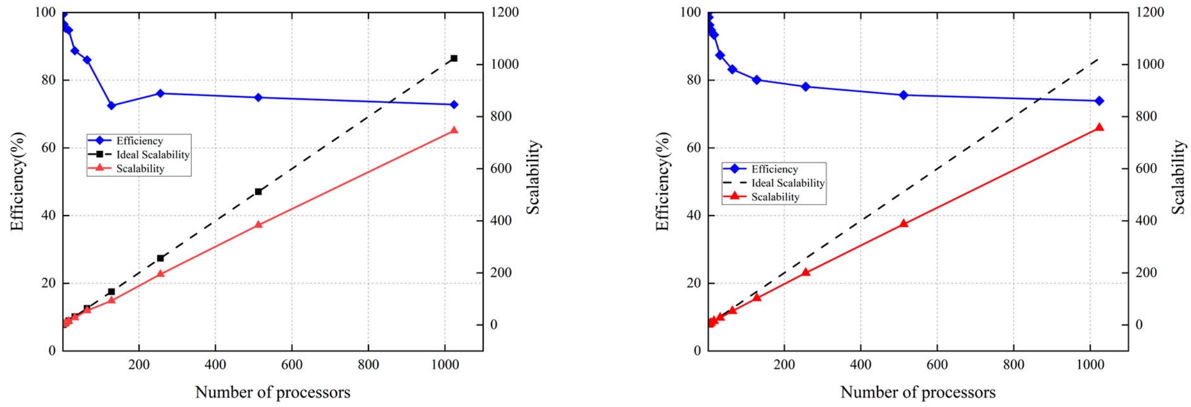

(**a**) (**b**)

Figure 12. (**a**) The parallel scalability and efficiency of the 100-period folded waveguide on a multi-node; (**b**) the parallel scalability and efficiency of the 16 × 16 phased array antenna on a multi-node.

4. Discussion and Conclusions

The FDTD algorithm is a commonly used numerical method in electromagnetic fields. It enjoys advantages of easy understanding and simple implementation, wide application, high precision under reasonable grid resolutions, and good stability under CFL conditions. However, when it comes to complex structure and large size problems, the number of grids will become very large, and the traditional FDTD algorithm obviously cannot bear such a huge computational burden.

In order to solve the above problems, a parallel FDTD method based on non-uniform conformal mesh is introduced. We use virtual mesh to exchange magnetic field information in adjacent subregions, and the electric field update is divided into inner and outer parts; moreover, the magnetic field exchange and internal electric field update are carried out at the same time. In this method, the whole iteration process is interrupted only once, which can be easily extended to the CPML absorption boundary and can realize the unification of internal electromagnetic field update formulas and PML update formulas; thus, it is very suitable for parallelization and avoids unnecessary data transmission. We test the parallel effects of a single node and multi-node on the supercomputing platform. It is shown that when the number of processors is small, especially with the single node, the parallel efficiency is higher than 90% and the acceleration ratio is close to linearity; however, with the increase in the number of processors, the cross-node communication time involved will also rise, and the parallel efficiency will decrease, but the overall parallel effect is good, which can effectively solve large-scale computing problems.

5. Recommendation

In this paper, a parallel FDTD method based on non-uniform conformal mesh is proposed, which can greatly reduce the computational burden and solve large-scale problems effectively, but there are still some aspects worth further exploration.

In the process of region decomposition, we try our best to ensure the uniform distribution of computation in each subregion and reduce the amount of data transmission, and perform load balancing to improve the parallel performance. By designing a more efficient load balancing strategy, such as one highly associated with CPU and other hardware, realizing the dynamic scheduling of processors, and using a parallel coloring method, the processor performance can be fully utilized, and the parallel efficiency can be further improved. In addition, the use of a hybrid parallel strategy, such as combining GPU parallel methods, so that it can be applied to large-scale simulation scenarios, including large-scale phased array antennas, system-level electromagnetic compatibility, and simulation applications based on realistic scenarios, is a feasible direction for future work.

Author Contributions: Conceptualization, K.L.; methodology, K.L.; software, K.L., G.L., L.H., W.C. and C.F.; data curation, K.L.; validation, K.L, G.L. and L.H.; data curation, K.L.; writing—original draft preparation, K.L.; writing—review and editing, X.J.; project administration, T.H., L.Z. and D.G. All authors have read and agreed to the published version of the manuscript.

Funding: This research received no external funding.

Institutional Review Board Statement: Not applicable.

Informed Consent Statement: Not applicable.

Data Availability Statement: The data presented in this study are available on request from the corresponding author. The data are not publicly available due to privacy.

Acknowledgments: Thanks to Chengdu Huangfeng Technology Co., Ltd. for providing the electromagnetic field simulation software 'BUMBLEBEE v1.0'.

Conflicts of Interest: The authors declare no conflicts of interest.

References

1. Yee, K. Numerical solution of initial boundary value problems involving Maxwell's equations in isotropic media. *IEEE Trans. Antennas Propag.* **1966**, *14*, 302–307. [CrossRef]
2. Monk, P.; Süli, E. A convergence analysis of Yee's scheme on nonuniform grids. *SIAM J. Numer. Anal.* **1994**, *31*, 393–412. [CrossRef]
3. Taflove, A.; Brodwin, M.E. Numerical solution of steady-state electromagnetic scattering problems using the time-dependent Maxwell's equations. *IEEE Trans. Microw. Theory Tech.* **1975**, *23*, 623–630. [CrossRef]
4. Cangellaris, A.C.; Wright, D.B. Analysis of the numerical error caused by the stair-stepped approximation of a conducting boundary in FDTD simulations of electromagnetic phenomena. *IEEE Trans. Antennas Propag.* **1991**, *39*, 1518–1525. [CrossRef]
5. Dey, S.; Mittra, R. A locally conformal finite-difference time-domain (FDTD) algorithm for modeling three-dimensional perfectly conducting objects. *IEEE Microw. Guid. Wave Lett.* **1997**, *7*, 273–275. [CrossRef]
6. Gedney, S. *Introduction to the Finite-Difference Time-Domain (FDTD) Method for Electromagnetics*; Springer Nature: Berlin/Heidelberg, Germany, 2022.
7. Xiao, T.; Liu, Q.H. A 3-D enlarged cell technique (ECT) for the conformal FDTD method. *IEEE Trans. Antennas Propag.* **2008**, *56*, 765–773. [CrossRef]
8. Xiao, T.; Liu, Q.H. Enlarged cells for the conformal FDTD method to avoid the time step reduction. *IEEE Microw. Wirel. Compon. Lett.* **2004**, *14*, 551–553. [CrossRef]
9. Zagorodnov, I.; Schuhmann, R.; Weiland, T. Conformal FDTD-methods to avoid time step reduction with and without cell enlargement. *J. Comput. Phys.* **2007**, *225*, 1493–1507. [CrossRef]
10. Roden, J.A.; Gedney, S.D. Convolution PML (CPML): An efficient FDTD implementation of the CFS–PML for arbitrary media. *Microw. Opt. Technol. Lett.* **2000**, *27*, 334–339. [CrossRef]
11. Gedney, S.D. An anisotropic perfectly matched layer-absorbing medium for the truncation of FDTD lattices. *IEEE Trans. Antennas Propag.* **1996**, *44*, 1630–1639. [CrossRef]
12. Berenger, J.P. A perfectly matched layer for the absorption of electromagnetic waves. *J. Comput. Phys.* **1994**, *114*, 185–200. [CrossRef]
13. Varadarajan, V.; Mittra, R. Finite-difference time-domain (FDTD) analysis using distributed computing. *IEEE Microw. Guid. Wave Lett.* **1994**, *4*, 144–145. [CrossRef]
14. Gedney, S.D. Finite-difference time-domain analysis of microwave circuit devices on high performance vector/parallel computers. *IEEE Trans. Microw. Theory Tech.* **1995**, *43*, 2510–2514. [CrossRef]
15. Liu, Y.; Mittra, R.; Su, T.; Yang, X.; Yu, W. *Parallel Finite-Difference Time-Domain Method*; Artech: Morristown, NJ, USA, 2006.
16. Yu, W.; Yang, X.; Liu, Y.; Ma, L.C.; Sul, T.; Huang, N.T.; Mittra, R.; Maaskant, R.; Lu, Y.; Che, Q.; et al. A new direction in computational electromagnetics: Solving large problems using the parallel FDTD on the BlueGene/L supercomputer providing teraflop-level performance. *IEEE Antennas Propag. Mag.* **2008**, *50*, 26–44. [CrossRef]
17. Guiffaut, C.; Mahdjoubi, K. A parallel FDTD algorithm using the MPI library. *IEEE Antennas Propag. Mag.* **2001**, *43*, 94–103. [CrossRef]
18. Kuo, C.M.; Kuo, C.W. A novel FDTD time-stepping scheme to calculate RCS of curved conducting objects using adaptively adjusted time steps. *IEEE Trans. Antennas Propag.* **2013**, *61*, 5127–5134. [CrossRef]
19. Gu, X. *Fast PIC Simulation Research of New Vacuum Electronic Devices*; University of Electronic Science and Technology of China: Chengdu, China, 2020. [CrossRef]